Simulated retreat of Jakobshavn Isbræ during the 21st century

Xiaoran Guo[1], Liyun Zhao[1,5], Rupert Gladstone[2], Sainan Sun[3], John C. Moore[1,2,4]
[1]College of Global Change and Earth System Science, Beijing Normal University, Beijing 100875, China
[2]Arctic Centre, University of Lapland, P.O. Box 122, 96101 Rovaniemi, Finland
[3]Laboratoire de Glaciologie, Université libre de Bruxelles, Brussels, Belgium
[4]CAS Center for Excellence in Tibetan Plateau Earth Sciences, Beijing 100101, China
[5]Southern Marine Science and Engineering Guangdong Laboratory (Zhuhai), China

Correspondence to: John C. Moore (john.moore.bnu@gmail.com)

Abstract

The early 21st century retreat of Jakobshavn Isbræ, into its over-deepened bedrock trough was accompanied by acceleration to unprecedented ice-stream speeds. Such dramatic changes suggested the possibility of substantial mass loss over the rest of this century. Here we use a three-dimensional ice-sheet model with parameterizations to represent the effects of ice mélange buttressing, crevasse-depth-based calving and submarine melting, to adequately reproduce its recent evolution. We are the first study on Jakobshavn Isbræ that solves for three-dimensional ice flow coupled with representations of hydro-fracturing induced calving and mélange buttressing. Additionally, the model can accurately replicate inter-annual variations in grounding line and terminus position, including seasonal fluctuations that emerged after arriving at the over-deepened basin and the disappearance of its floating ice shelf. Our simulated ice viscosity variability due to shear margin evolution is particularly important in reproducing the large observed inter-annual changes in terminus velocity. We use this model to project Jakobshavn's evolution over this century forced by

ocean temperatures from 7 Earth System Models and surface runoff derived from RACMO, all under the IPCC RCP4.5 climate scenario. In our simulations, Jakobshavn's grounding line continues to retreat ~ 18.5 km by the end of this century leading to a total mass loss of ~ 2068 Gt (5.7 mm sea level rise equivalent). Despite the relative success of the model in simulating the recent behavior of the glacier, the model does not simulate winter calving events that have become relatively more important.

1 Introduction

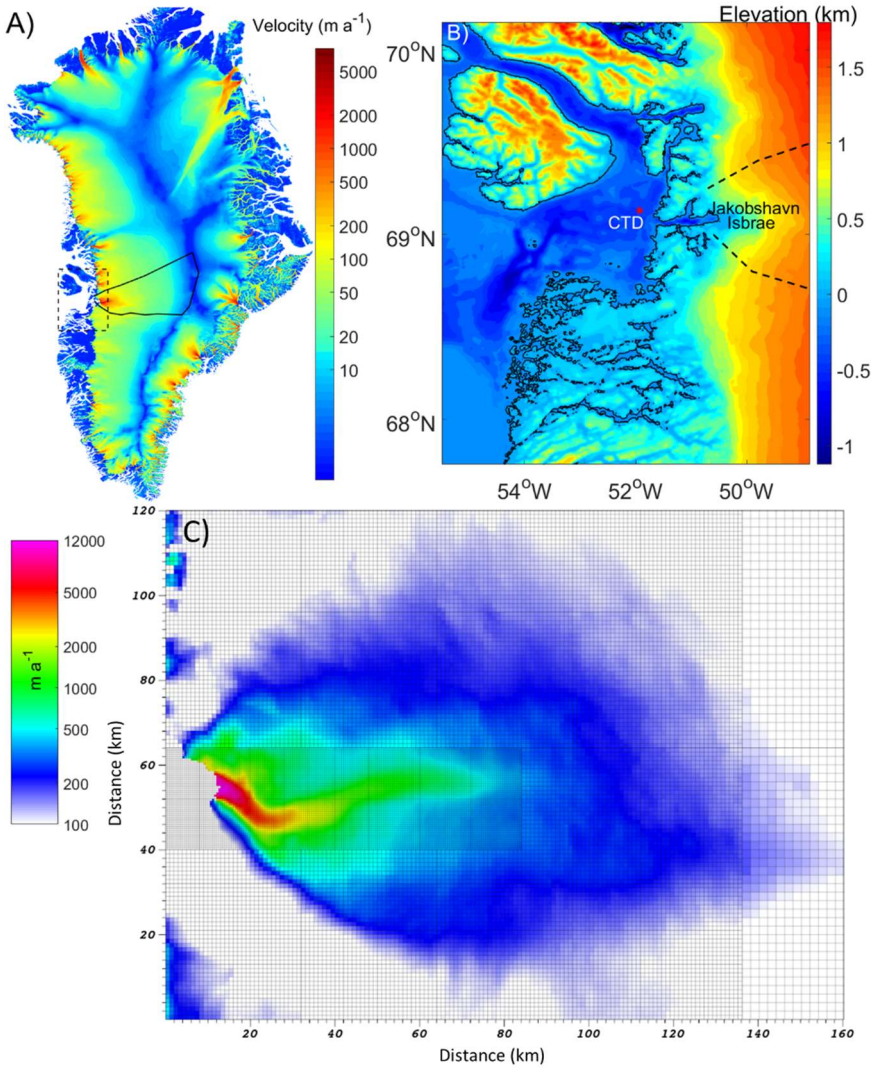

Figure 1. A) Greenland ice sheet flow speeds from Joughin et al. (2018), with the

Jakobshavn drainage basin outlined by the solid black line and the area shown in panel B by the dashed box. B) Ilulissat Fjord and Disko Bay bathymetry from Jakobsson et al. (2012), with the CTD (Conductivity Temperature Depth) site used for ocean temperature here marked by the red star. C) Example of the mesh used with finest resolution of 500 m with modeled velocities at the beginning of 2004.

Jakobshavn Isbræ (Fig. 1) is Greenland's largest and fastest outlet glacier, with transient speeds of up to 17 km a^{-1} (Joughin et al., 2014). Jakobshavn Isbræ drains ~ 6.5 % of the Greenland Ice sheet (Krabill et al., 2000), and it alone contributed ~ 1 mm to global sea-level rise between 2000 and 2011 (Howat et al., 2011). Since 1997, measurements indicate that the water entering Ilulissat Fjord where Jakobshavn Isbræ terminates, is about 1.1 ºC warmer than it was during 1987-1991 (Holland et al., 2008). This rise in water temperature coincided with the onset of dramatic thinning, speedup and retreat of Jakobshavn Isbræ. By 2003 its velocity near the grounding line had reached ~ 12.6 km a^{-1}, more than double that of 1992, and the ice shelf in the fjord had disintegrated (Joughin et al., 2004). From 2005 to 2007, as it retreated inland, seasonal fluctuations in velocity 4 km inland from the calving front amounted to $\pm$ 1 km a^{-1}. The winter slowdowns and summer accelerations occurred in tandem with the calving front winter advance and summer retreat. By 2012 the seasonal velocity fluctuations 4 km upstream from the calving front were nearly ± 8 km a^{-1} and the grounding line of Jakobshavn Isbræ had reached the bottom of a sub-glacial bedrock trough after years of down-slope migration (Joughin et al., 2014).

Before 1997, Jakobshavn had a ~ 15 km long ice shelf in front of its grounding line and experienced submarine melting on its ice-ocean interface (Amundson et al., 2010). After 1998 the terminus became more crevassed, coinciding with acceleration of the glacier, implying that weakened buttressing had triggered its dramatic speed-up. A thinning rate of 230 ± 50 m a^{-1} between the summers of 1984 and 1985 was deduced from photogrammetric surveys, with 98% contributed by submarine melting (Motyka et al., 2011). The ice shelf thickened during the mid-1990s followed by

progressive thinning after 1997 (Motyka et al., 2011). From 1997 to 2008, the average ocean temperature was 1.1°C higher than during the period 1980 – 1991, which raised its thinning rate substantially, affecting the whole ice shelf that eventually collapsed in 2003. Many lines of evidence suggest that warm water was responsible for the submarine melting beneath the ice mélange and ice-shelf, brought by a buoyancy-driven, overturning circulation in Ilulissat fjord (Gladish et al., 2015).

Jakobshavn, in common with most outlet glaciers in Greenland, flows through a narrow, deeply incised bedrock trough at a much faster rate than the ice surrounding it (Joughin et al., 2010). Gravity surveys suggest a deep layer of soft till underlies much of the Jakobshavn trough (Block and Bell, 2011). This soft bed provides almost no resistance to ice flow and basal shear stress maps show that most of the gravitational driving force on the glacier is balanced by lateral drag (Shapero et al., 2016).

Basal drag decreased from 1995 to 2006 (Habermann et al., 2013), possibly due to fast thinning that reduced the effective pressure, that is the ice overburden minus water pressure, at the bed. The effective pressure distribution under the glacier is important to basal drag and approaches zero at the grounding line as the ice begins to float. Several sliding parameterizations (also termed sliding relations or sliding laws) have been used in the literature that assume basal drag depends on sliding speed (so-called Weertman sliding (Weertman, 1957)), or on effective pressure (Schoof, 2010; Gagliardini et al., 2014). Tsai et al. (2015) introduced a combined Weertman and Coulomb sliding law based on effective pressures with a boundary layer at the grounding line; this has a higher scaling of ice flux with grounding-line thickness compared with the Weertman. However, in the Jakobshavn case, both Weertman and Coulomb sliding produce very similar fluxes because the basal shear stresses along the main trough are typically only 2% of the driving force (Shapero et al., 2016).

Simulations using a flow-band model with a crevasse-depth-based calving parameterization (Vieli et al., 2011) demonstrated that loss of buttressing from the weakening mélange or enhanced submarine melting could have triggered the dramatic changes seen in Jakobshavn Isbræ at the end of the 20th century. Later work (Muresan et al., 2016), using a simple calving model with dependence on the strain field at the terminus was able to reproduce the inter-annual retreat of Jakobshavn Isbræ until 2009, when the terminus arrived at the beginning of the reverse sloping bed. But retreat after 2010 was not captured by their model, and neither were the seasonal fluctuations in terminus position. Bondzio et al. (2018) applied a similar calving model that removes any ice where tensile stress exceeds a threshold, as simulated with a SSA (Shallow Shelf Approximation) model, regardless of ice thickness. To represent seasonal fluctuation of front position, their stress threshold is a stepwise constant function in time with low values in summer. After calibration, their model can closely reproduce the observed behavior from 1985 to 2018 when forced only with ocean temperatures.

In this paper we use a three-dimensional ice-flow model with a treatment of calving that successfully tracks the seasonal terminus position and its retreat into the over-deepened basin. We use historic observations of ocean temperature as forcing and ice shelf melting rate to scale submarine melting rates for our model and thence make future projections. Our aim is to track the evolution of Jakobshavn Isbræ through the 21st century under a specific climate forcing scenario. In Section 2 we describe the approach and calibration of our model, Section 3 shows the simulations for the period to 2100 under the IPCC RCP4.5 scenario (Moss et al., 2010), Section 4 is a discussion of our results with reference to other studies and suggestions for improvements, and we conclude in Section 5.

2 Methods and data

2.1 Ice sheet model

We model Jakobshavn Isbræ using the BISICLES ice sheet dynamics model that is based on the vertically integrated stress balance formulation of Schoof and Hindmarsh (2010), which treats longitudinal and lateral stresses as depth-independent, but allows for vertical shear in the nonlinear rheology (Cornford et al., 2013). BISICLES is particularly useful for Jakobshavn Isbræ as it uses block-structured finite volume discretization with adaptive mesh refinement (Cornford et al., 2013) allowing for high resolution modeling of critical sections of the glacier. Jakobshavn Isbræ is fed by a ~ 400 km long and extensive drainage basin (Fig. 1), but the fast flow area is only around 10 km in width. Our highest mesh resolution of 500 m is used to cover the whole fast-flow-area including the shear margin (Fig. 1c), while the rest of the glacier is modeled at 1000 m resolution.

We assume the floating part of Jakobshavn Isbræ to be in hydrostatic equilibrium, thus the upper surface elevation s is

$$s = \max\left[h + b, \left(1 - \frac{\rho_i}{\rho_w}\right) h\right], \quad (1)$$

where ρ_i and ρ_w are the densities of ice (917 kg m^{-1}) and ocean water (1027 kg m^{-1}), h is ice thickness and b is bedrock elevation relative to sea level. The ice thickness evolves in time as

$$\frac{\partial h}{\partial t} + \nabla \cdot [\boldsymbol{u}h] = M_s - M_b, \quad (2)$$

where M_s, M_b are surface mass balance (SMB) and submarine melt rate respectively and $\boldsymbol{u}$ is the depth-independent horizontal velocity. No basal melting over the grounded area is allowed. The velocity $\boldsymbol{u}$ satisfies an approximate stress balance equation (Schoof and Hindmarsh, 2010)

$$\nabla \cdot [\phi h\bar{\mu}(2\dot{\boldsymbol{\epsilon}} + 2\mathrm{tr}(\dot{\boldsymbol{\epsilon}})\mathbf{I})] - \boldsymbol{\tau}^b = \rho_i g h \nabla s, \quad (3)$$

where $\mathbf{I}$ is the identity tensor, s is the ice surface elevation, g is the acceleration due to gravity, $\dot{\boldsymbol{\epsilon}}$ is the horizontal strain-rate tensor defined by

$$\dot{\boldsymbol{\epsilon}} = \frac{1}{2}[\nabla \boldsymbol{u} + (\nabla \boldsymbol{u})^{\mathrm{T}}], \quad (4)$$

and $\boldsymbol{\tau}^b$ is the basal shear stress. The vertically integrated effective viscosity $h\bar{\mu}$ is given by

$$h\bar{\mu}(x, y) = \int_{s-h}^{s} \mu(x, y, z)\mathrm{dz}, \quad (5)$$

where the vertically varying effective viscosity μ includes a contribution from vertical shear and satisfies

$$2\mu A(T)(4\mu^2\dot{\boldsymbol{\epsilon}}^2 + |\rho_i g(s - z)\nabla s|^2)^{(n-1)/2} = 1, \quad (6)$$

where n is the flow rate exponent, set to 3 in the current study, and $A(T)$ is the rate factor, dependent on the ice temperature T through an Arrhenius law (Cuffey and Paterson, 2010). ϕ is a stiffening factor estimated by solving an inverse problem (Cornford et al., 2015) using measured surface velocities.

We use a viscous Weertman sliding relation to define the basal friction:

$$\boldsymbol{\tau}^b = \begin{cases} -C|\boldsymbol{u}|^{m-1}\boldsymbol{u} & \text{if} \frac{\rho_i}{\rho_w} h > -b \\ 0 & \text{otherwise} \end{cases}, \quad (7)$$

and here we assume a linear relation taking m=1. The basal traction coefficient C(x, y) is estimated simultaneously with the stiffening factor ϕ by solving the inverse problem (Cornford et al., 2015). C and ϕ are adjusted iteratively to reduce the misfit with a set of 2010 surface velocity observations (Joughin et al. 2010). We hold the fields C and ϕ constant over time throughout our simulations,

137 although they must actually change as the glacier retreats. We also do not thermomechanically

138 couple the model, but use a constant ice temperature of -10°C.

139 Reflection boundary conditions were applied at the edge of the domain:

140 $$\boldsymbol{u}\cdot\boldsymbol{n}=0,\qquad \boldsymbol{t}\cdot\nabla\boldsymbol{u}\cdot\boldsymbol{n}=0,\qquad \nabla h\cdot\boldsymbol{n}=0, \quad (8)$$

141 where $\boldsymbol{n}$ is normal to a boundary and $\boldsymbol{t}$ is parallel to it. Normal stress across the calving front is equal

142 to the hydrostatic water pressure there:

143 $$\boldsymbol{n}\cdot[\phi h\bar{\mu}(2\dot{\boldsymbol{\epsilon}}+2\mathrm{tr}(\dot{\boldsymbol{\epsilon}})\mathbf{I})]-\boldsymbol{\tau}^{b}=\frac{1}{2}\rho_i \mathrm{g}\left(1-\frac{\rho_i}{\rho_w}\right)h^2\boldsymbol{n}. \quad (9)$$

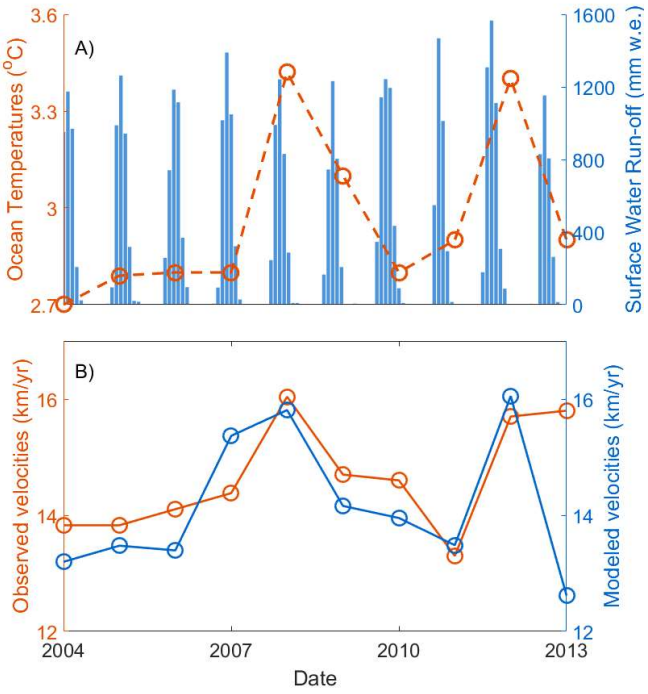

144

145 **Figure 2. A) Time series of observed ~300 m deep ocean temperature (red) from near the mouth of**
146 **Ilulissat fjord (See Fig. 1 for location). Blue bars are simulated monthly surface water run-off from**
147 **the MAR regional surface mass and energy balance model (Alexander et al. 2016). B) Measured**
148 **ice front annual mean ice flow speeds (red) from Joughin et al. (2010), compared with our modeled**
149 **speeds (blue).**

2.2 Forcing

Local ocean circulation in Ilulissat fjord driven by buoyancy plume brings deep water from outside to the grounding line of Jakobshavn, and renews the fjord waters within 90 days in summer (Gladish et al., 2015). Generally, Jakobshavn's fjord is ~ 800 m deep but with a sill of only ~ 200 m depth at its entrance. The deepest water outside the sill can flow over the sill and reach the grounding line of Jakobshavn (Gladish et al., 2015). We use 300 m depth ocean temperatures collected from a CTD site close to the mouth of Ilulissat fjord (Fig. 1) as an approximation of ocean temperatures near the glacier grounding line (Gladish et al. 2015). A positive correlation ($r=0.74$, $p<0.05$) exists between deep ocean temperatures and flow speed near the terminus of Jakobshavn Isbrae (Fig. 2) from 2004 onwards. There is no significant correlation prior to 2004, the ice shelf period. As a working hypothesis we assume that the correlation since 2004 reflects the effects of the sea ice and iceberg mélange in the fjord on the flow speed near the terminus: a warmer ocean reduces mélange and sea ice thickness and therefore buttressing. There appears to be no lag between the glacier acceleration and change in deep ocean temperature, suggesting mélange response times are faster than 1 year. When the ice shelf was present lags in the system were likely longer, accounting for the lack of correlation between ocean temperatures and glacier flow speed prior to 2004. It is also possible that ocean temperatures reflect changes in surface runoff and basal lubrication for sliding, but we consider that the runoff more strongly affects calving mechanisms as discussed later. We therefore modify the driving force (Eq. 3) on the grid cells next to the calving front by multiplying by a factor α that is linearly related to ocean temperature (T) as a means of representing the buttressing effects of the ice mélange in the fjord.

$$\nabla \cdot [\phi h \bar{\mu}(2\dot{\boldsymbol{\epsilon}} + 2\mathrm{tr}(\dot{\boldsymbol{\epsilon}})\mathbf{I})] + \boldsymbol{\tau}^b = \alpha \cdot \rho_i g h \nabla s, \quad (10)$$

$$\alpha = \alpha_1 + \alpha_2 \cdot T, \quad (11)$$

The coefficients α_1 and α_2 are tunable with limits based on observations as discussed later in Section 2.4. This approach is similar to Nick et al. (2013), which also alters the stress balance at calving front. Our buttressing parameterization gives a longitudinal resistance that is 18% of the driving force at calving front (Eq. 10), for the instance of 2004.

We use a crevasse based calving parameterization (Benn et al., 2007; Nick et al., 2013) that calves ice where the crevasse penetration depth (D_s) is greater than upper surface elevation. D_s is defined as

$$D_s = \frac{S}{g \cdot \rho_i} + \frac{\rho_w}{\rho_i} \cdot \mathrm{R} \cdot \beta, \quad (12)$$

where S is the magnitude of extensional stress, R is surface water run-off, and β is a tuning scalar. We estimate runoff from the 25 km resolution regional climate model, MAR, (Alexander et al. 2016), driven by the ERA-Interim reanalysis (Dee et al., 2011).

We characterize submarine melting as a linear function of ocean forcing

$$M_b = \gamma\, T_{f,} \quad (13)$$

where T_f is the far field ocean forcing temperature, taken in Disko Bay (CTD in Fig. 1), relative to pressure melting temperature under the ice shelf. Thus T and T_f are related simply by ice depth and salinity. We derive γ (Section 2.3) from the 1985 observed submarine melt rate of 1 ± 0.2 m day^{-1} beneath the ice shelf of Jakobshavn Isbræ, when Disko Bay ocean temperatures were 4.2°C warmer than the pressure melting point at the bottom of the floating ice shelf (Motyka et al. 2011). We test the sensitivity of the modeled glacier to uncertainty in submarine melt rate in section 2.4.

We force Jakobshavn Isbræ in the 21st century using SMB and run-off from the 11 km resolution RACMO model (Van Angelen et al., 2013) driven by the RCP4.5 scenario (Moss et al. 2010). The

194 run-off values are averaged over the nine grid points nearest to the terminus of Jakobshavn (69.1°N,
195 50.0°W). In general we use RACMO products to drive the model, however they only span the period
196 of 2006-2099. For the period 2004-2014, SMB and surface water run-off forcing come from MAR
197 model outputs. We use the common overlap period (2006-2014) to correct the bias between two
198 models outputs. The RACMO simulation was forced by the HadGEM2-ES Earth system model
199 (Collins et al., 2011), as this climate model was found to be the most realistic for present-day
200 simulations of the Greenland ice sheet (Van Angelen et al., 2013). Ocean forcing in Equations (10)
201 and (13) should relate to temperatures off the continental shelf close to the fjord mouth. Cowton et
202 al. (2018) achieved success in simulating the terminus position and yearly variability of 10 glaciers
203 along the east coast of Greenland using mean 200-400 m depth temperatures from reanalysis data.
204 For consistency with the RACMO results, we use deep ocean temperatures at ~ 300 m depth from
205 the 0.83°×1° resolution HadGEM2-ES driven by the RCP 4.5 climate scenario from 2005 to 2100
206 at the 3 closest grids point to Disko Bay. We also compare this with results from 7 other climate
207 model simulations of RCP4.5: HadGEM2-ES (Collin et al., 2011), BNU-ESM (Ji et al., 2014),
208 MIROC-ESM (Watanabe et al., 2011), IPSL-CM5A-LR (Dufresne et al., 2013), CSIRO-Mk3L-1-2
209 (Gordon et al., 2002), NorESM1-M (Bentsen et al., 2012) and MPI-ESM-LR (Giorgetta et al., 2013).

210 2.3 Initialization Procedure

211 As we are interested in high resolution simulations and validating our model parameterizations with
212 observations over the last decade, we take care to initialize the model as accurately as possible.
213 Detailed bedrock topography and ice thickness data in the year 2009 comes from Gogineni et al.
214 (2012); we chose the product because it has 500 m resolution and so matches the highest resolution
215 of our mesh. Jakobsson et al. (2012) provides ocean bathymetry data (Fig. 1). In 2004 the floating
216 ice shelf disintegrated, making it a convenient starting point for simulations since we might expect

the system to respond differently to forcing when there was a floating ice shelf compared with the situation of ocean forcing along a near-vertical ice cliff. This is consistent with the observed good correlation between ocean temperature and flow speed after 2004 but not before. The aim of this initialization is to provide a state rather similar to 2004, that is barely retreating on inter-annual scales (Joughin et al., 2010) and small changes of annual mean velocity in the following 3 years. Therefore

1) We solved the inverse problem for basal conditions (Eq. 7) and stiffening factor using 2010 velocities (Joughin et al., 2010) and 2009 geometry (Gogineni et al., 2012), following Cornford et al. (2015). Our friction coefficient and stiffening factor fields are shown in Fig. 3. Fig. S1 shows the discrepancy between observed velocity field (Joughin et al., 2010) and the velocity derived from the inversion.

2) Starting from the inversion of step 1, we let the model glacier evolve freely without calving and with zero SMB and with sub-shelf melting (γ=0.0238) forced by repeating the observed 2004 ocean temperature for 11 years until its surface elevation profile reached a state shown in Fig. S2.

3) We carried out several 10-year simulations each with different β values. These simulations were forced by repeatedly applying the 2004 seasonal climate forcing so that the glacier approaches a steady state. From these, we selected the β that provided a calving front position closest to that observed in 2004. The best β here is 0.034, and this is our best guess for the 2004 state. The annual minimum extent of Jakobshavn retreats ~ 2 km from 2004 to 2005 following the loss of ice shelf butressing, but then stabilizes until 2007 (Joughin et al. 2010). Annual maximum extents are stable over the 2004-2007 period. Front velocity increase slowly from 2004-2007 (~5.9% a^{-1} Joughin et al. 2010), and the model simulated velocities increase by

about 3% a^{-1}. This period of relative stability also makes 2004 a good time from which to start transient simulations.

Basal friction coefficient values downstream of the 2010 grounding line were set equal to that in the nearest 2010 grounded location. This was necessary because steps 2 and 3 involved grounding line advance beyond the region for which basal friction coefficients had been inferred. The geometry after this spin up procedure, and the friction coefficient and stiffening factor distribution from the inversion in step 1 were used as the initial condition for model calibration.

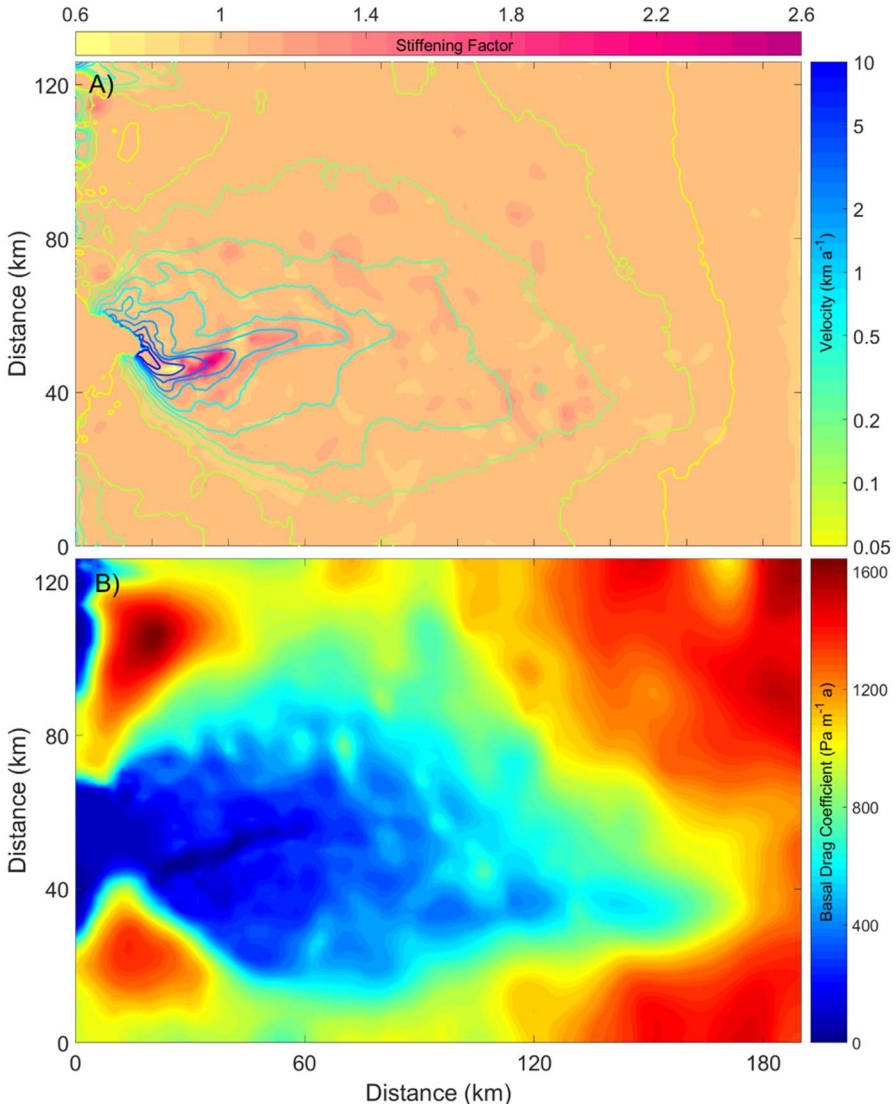

Figure 3. (A) Stiffening factor Φ (Eq. 3) and (B) basal traction coefficient C (Eq. 7) over the computational domain from solving the inverse problem. Contour lines in panel A show the modeled velocity (logarithmic scale).

2.4 Model calibration

The parameters in the model, α, β and γ representing mélange buttressing, crevasse depth sensitivity to surface runoff, and shelf melt sensitivity to ocean temperatures need to be estimated. The measured relationship between ocean temperatures and sub-shelf melt rate (Motyka et al., 2011) gives the value of γ to be 0.238. We manually tune parameters in equations (11) and (12): α over the range 0.7−1.2 for α_1 and 0.09-0.12 for α_2; and β (0.04 - 0.075) to best reproduce Jakobshavn Isbræ's calving front position and surface velocity evolution for the 10 year period 2004-2013. Reproducing the total retreat distance and the temporary stable state after 2012 were secondary desirable features to match. The best set of parameters are α_1=0.82, α_2=0.111, β=0.0638. Since these values come from a manual search we do not claim them to be the best in all parameter space. We assess model sensitivity to the parameter values next.

We explore the glacier's sensitivity to two types of boundary perturbations. They are ice mélange buttressing effect (defined by α) and submarine melting (defined by γ). We scaled submarine melt rates by multiplying it by values from 0.8-1.2, based on the range of the observation uncertainty in melt of ~ 20% (Motyka et al. 2011). Also we varied α by multiplying by factors from 0.91 to 1.25 to represent different buttressing strengths (Eq. 10). These multiplication factors were varied systematically with typical intervals of 0.1 and 0.03 respectively for the γ and α factors. We calculated the following relative mismatches defined as (model-observations)/observations for each simulation (Fig. 4):

1. Total calving front retreat from 2004-2013 measured by the difference between 2004 and

2013's annual maximum extent.

2. Annual mean front velocities

3. Vector sum of 1) and 2)

We used β (Eq. 12) from our optimal set of parameters. Our optimal value for α is such that a 20% rise of its value does not affect modeled retreat when β and γ are kept to be their optimal values (Fig. 4 A).

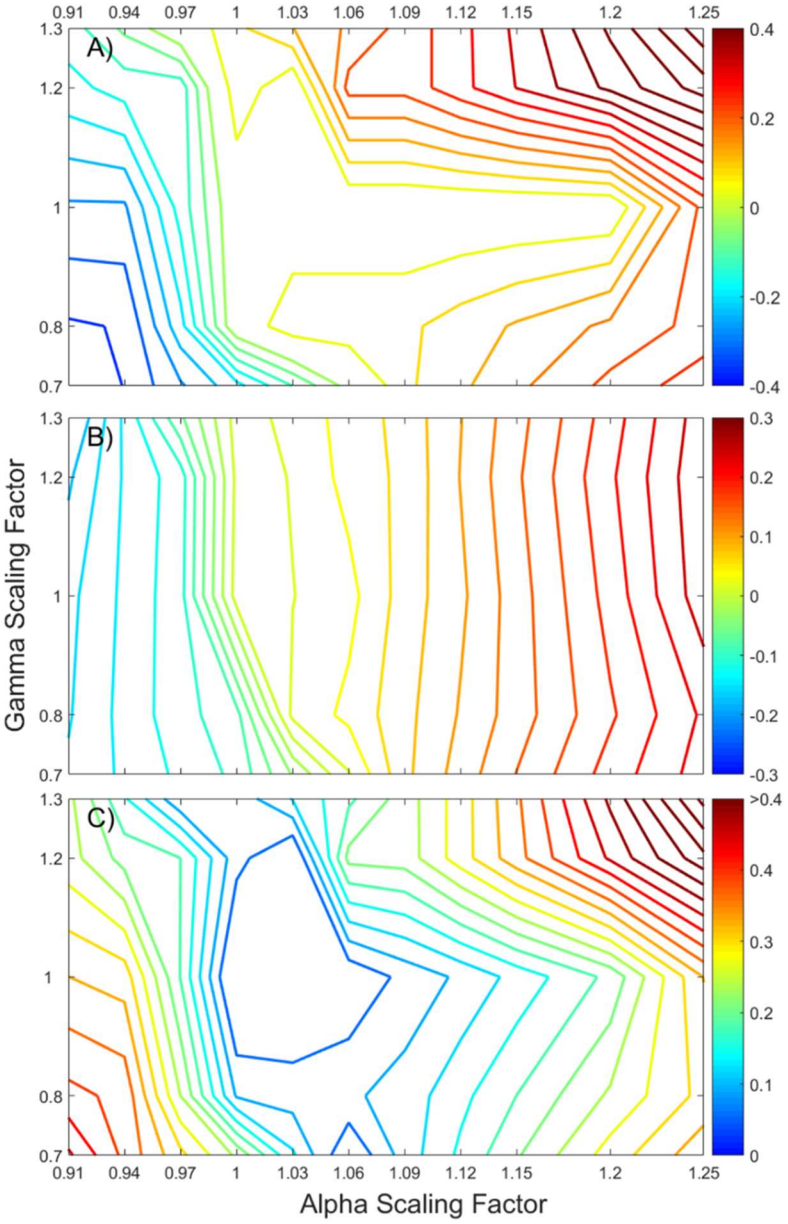

277

278 **Figure 4. Relative mismatches defined as (model-observed)/observed for A) total calving front**
279 **retreat, B) average of annual mean front velocity during 2004-2013, C) the vector sum of**
280 **mismatches in panels A and B, $\sqrt{(A^2 + B^2)}$ in our 2-D parameter space. X- and y-axis are**
281 **multipliers of α and γ.**

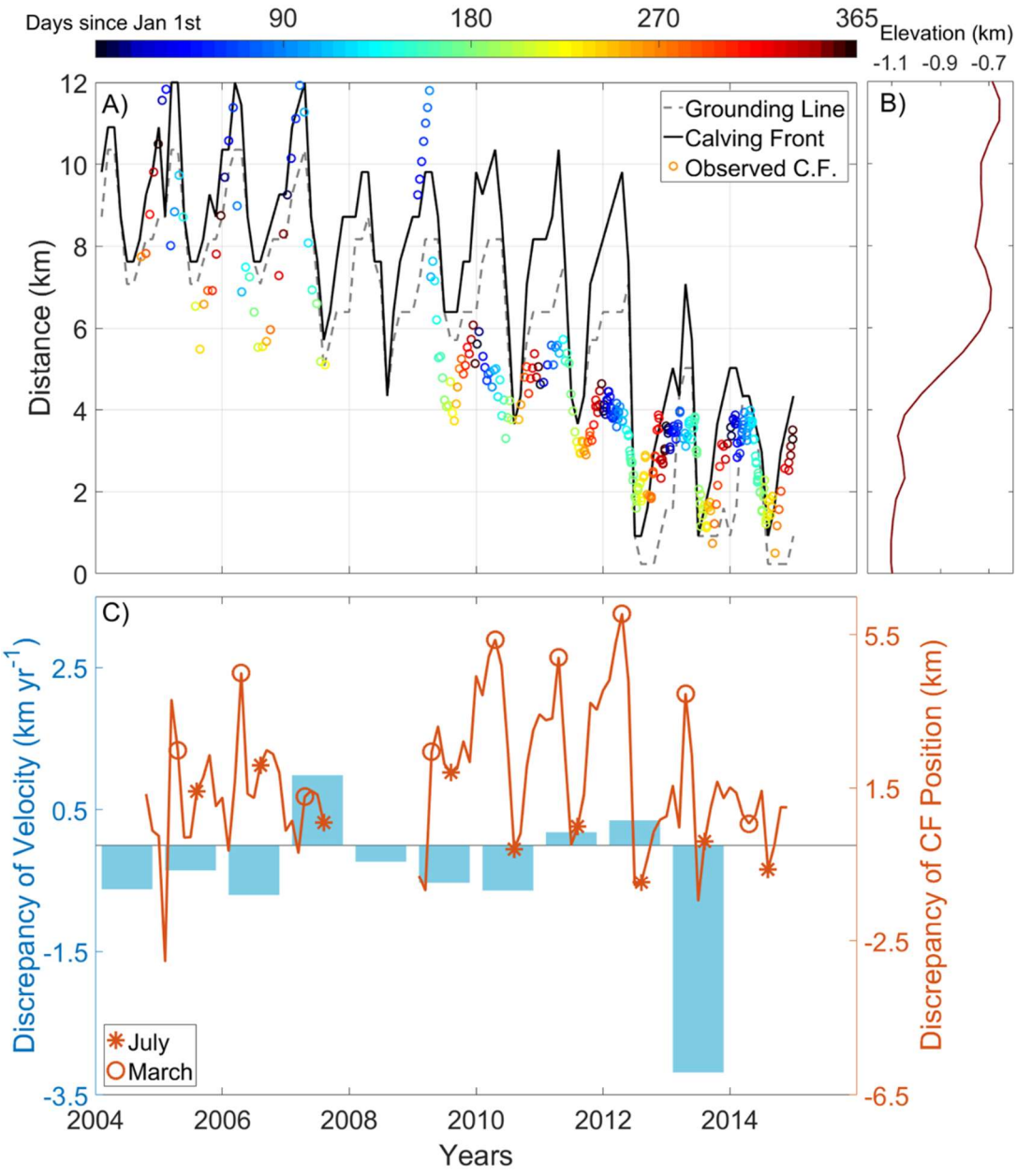

282

283 **Figure 5. (A) Modeled retreat of the calving front (black solid line), grounding line (gray**
284 **dashed line), and observed calving front positions (color-coded circles and scale bar) from**
285 **Joughin et al. (2014). (B) Bedrock elevations. (C) Residuals (modeled minus observed) of**
286 **annual mean front velocity (blue bars, left axis) and of calving front position (red lines, right**
287 **axis) with typical timings of annual maximum (March) and minimum (July) extent marked.**
288 **The modeled front velocities and calving positions explain about 49% and 76% of the variance**
289 **in corresponding observations.**

290 The two biggest mismatches occur with the 2007 and especially 2013 velocities (Fig. 5). 2013 has

291 the lowest simulated surface water run-off (Fig. 2) of all the years since 2004. The Benn calving

292 model we use is sensitive to runoff, with reduced run-off leading to lower crevasse-penetration-
293 depth and reduced terminus fracturing thus increasing its buttressing force. Furthermore 2013 had
294 relatively cool ocean temperatures which were lower than the average of 2004-2013. The cool ocean
295 temperatures also increased buttressing, leading to low simulated annual mean velocities.
296 Jakobshavn Isbræ did not in fact slow down very much in 2013 because there were calving events
297 (Cassotto et al. 2015) that are unrepresented in our model. The relevant mechanisms are discussed
298 later. In 2007 high run-off caused more simulated calving and retreat than in reality. These retreat
299 phases reduced the buttressing and lateral drag due to shear-margin-weakening, all of which lead to
300 excessive speed-up near the terminus.

301 Modeled calving front retreat is ~ 7 km in total from 2004-2014 (Fig. 5), which is consistent with
302 observations (Joughin et al. 2014). In 2009 a dramatic retreat brought the grounding line to the
303 bottom of the bedrock slope, and since then it has gradually retreated with smaller seasonal
304 fluctuations. The run-off forcing we applied triggered major retreats in the summers of 2007 and
305 2012, due to large summer peak run-off (Fig. 2), demonstrating the sensitivity of our calving
306 parameterization to run-off forcing. Modeled timings of maximum extent and minimum extent each
307 year are in good agreement with observations, also demonstrating that summer, in particular, May
308 to July, run-off determines much of the behavior of Jakobshavn Isbræ.

309 The modeled range of seasonal fluctuation in front position is ~ 5 km, which is similar to
310 observations in the period before 2008. From January 2009 to December 2011, there was an abrupt
311 decrease in seasonal front fluctuation, with many winter calving events occurring, in contrast with
312 previous years (Cassotto et al. 2015). These winter calving events may explain the small observed
313 seasonal fluctuations because they limit the winter advance. Our model is unable to stimulate these
314 winter calving events because there is no winter run-off, and as extension stresses are never enough

to cause winter calving, calving is then zero. The largest discrepancy of front position occurs during these winter calving periods (Fig. 5). Observations also showed that from 2013 to 2017, Jakobshavn Isbræ barely retreated (Joughin et al. 2010). The decline of run-off (Fig. 2) in 2014 suggests the reason. But since no RACMO run-off simulations are yet available for 2015 and later, our parameterizations cannot be tested against this lack of retreat.

3 Future evolution

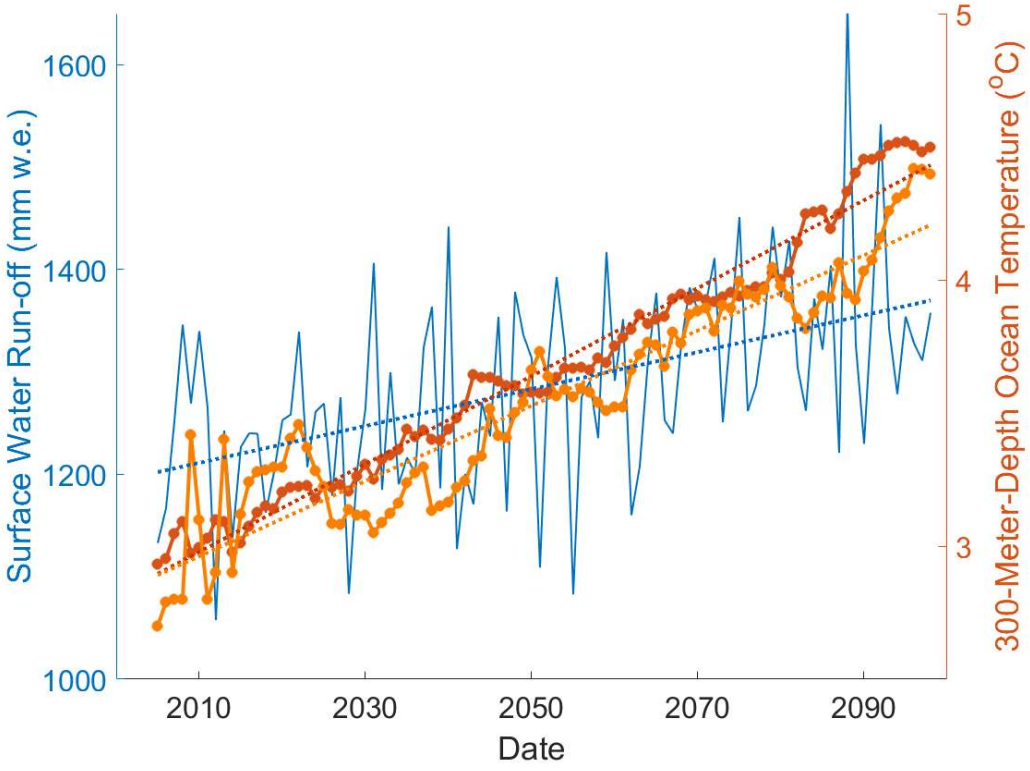

Figure 6. Climate forcing for future projection under the RCP4.5 scenario taken as 300 m depth ocean temperatures from HadGEM2-ES (orange) compared with the ensemble mean (red) of 7 Earth System Models (HadGEM2-ES, BNU-ESM, MIROC-ESM, IPSL-CM5A-LR, CSIRO-Mk3L-1-2, NorESM1-M and MPI-ESM-LR), (right axis), with their linear trends. Annual maximum monthly surface water run-off near Jakobshavn Isbrae's terminus from RACMO (forced by outputs from HadGEM2-ES) is shown in blue.

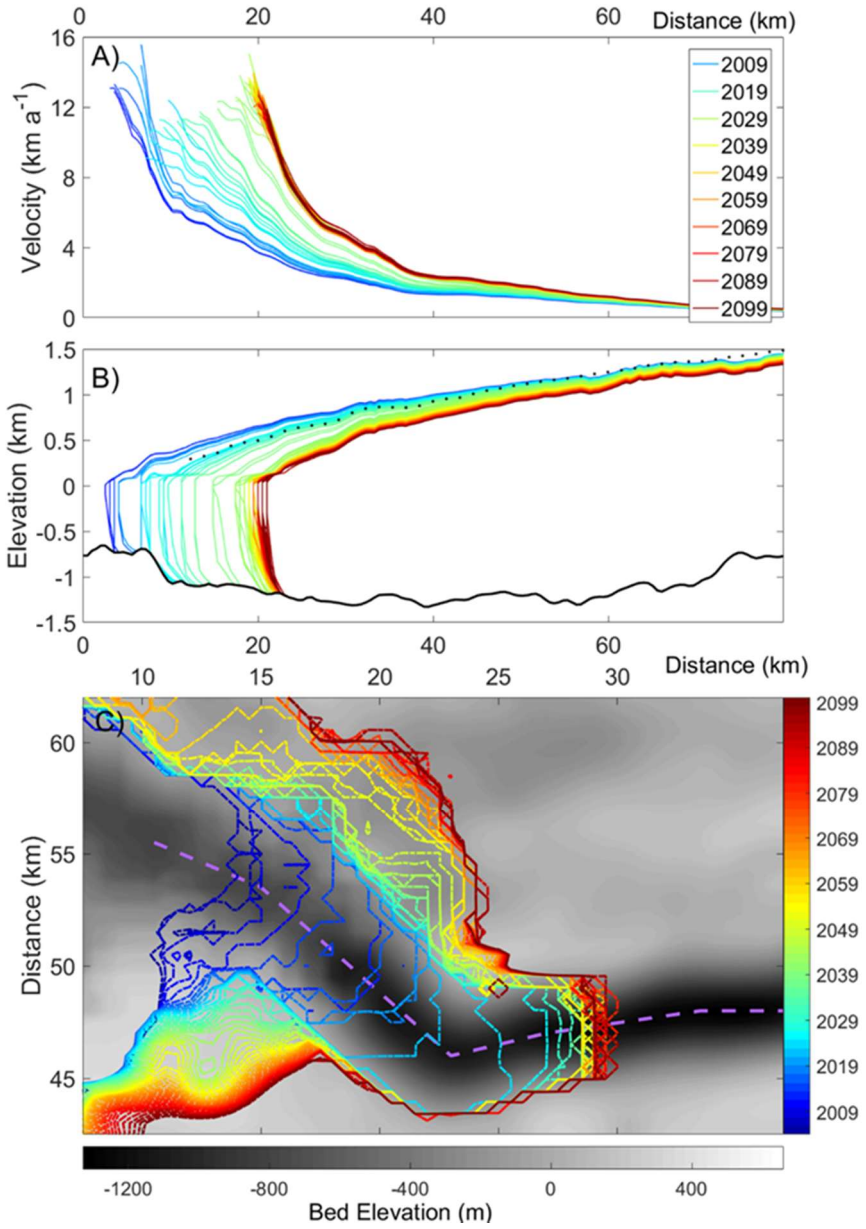

328

329 **Figure 7. Modeled profiles of (A) January velocity and (B) January surface elevation along**
330 **the center-flow-line (purple dash line in panel C) of Jakobshavn Isbræ from 2004 to 2099 for**
331 **the RCP4.5 scenario. Bedrock elevation is shown in black. Black dotted line is the surface**
332 **elevation profile extracted from radar data measured around 2010 (Gogineni et al., 2012).**
333 **Profiles are shown at intervals of 1 years. Profiles are color-coded in the legend and range**
334 **from blue to green and red. (C) Modeled July front positions (color bar) over its bedrock**
335 **(grayscale bar) at intervals of 2 years.**

336 Under the RCP4.5 scenario (Fig. 6) surface runoff slowly rises over the 21st century, with RACMO

337 simulating slightly greater runoff during the second half than for the first 50 years. Runoff increases

by 14% over the century. Ocean temperature at 300 m depth in the grid cell closest to Jacobshavn increases by 52%, and, as may be expected, has less variability than runoff.

Under this forcing, Jakobshavn Isbræ continues its retreat (Fig. 7) for 18 years after 2013, producing a total grounding line retreat of ~18 km upstream. As calving produces a steepening surface profile, terminus velocities increase, to reach a 21st century peak of ~19 km a^{-1} in 2031 summer. Eventually the front height (relative to sea level) becomes larger than the crevasse penetration depth in the calving parameterization. This leads to a stable period with little inter-annual retreat and which lasts until the end of this century. During this period, nearly all of the seasonal retreats are offset by the following winter re-advances. Mass transport continually flattens and thins the ice geometry, leading to reduced flow speeds that eventually become half those of 2031, the 21st century peak.

The surprisingly high run-off anomaly in 2088 (Fig. 6) does not affect the stable state indicating run-off fluctuation alone cannot break this retreat pattern immediately. Once the inter-annual retreats cease in 2031, the dynamic thinning rate is greatly reduced because calving front height stops increasing.

Table 1 Estimates of glacier mass loss and grounding line retreat from different sources.

Source	Climate scenario	Mass loss 2004-2013 (10 years) (Gt)	Mass loss by 2100 (Gt)	Grounding line retreat 2004-2013 (km)	Grounding line retreat by 2100 (km)
This paper	RCP4.5	234	2068 (2044-2723)	7.0	18.5 (17.5-23.0)
Muresan et al. (2016)		220			
Nick et al. (2013)	A1B		1870 - 2281		14.0 - 26.0
Observations		225±15		7.0	

Table 1 shows estimates of glacier mass loss and retreat. Under RCP4.5, total cumulative mass change of Jakobshavn Isbræ is 2068 Gt by 2100, using best set of α, β and γ with ocean temperature inputs from ensemble mean of 7 ESMs (Fig. 6). To estimate an upper bound for mass loss over this

356 century, we scale the α parameter by 1.2 giving 2680 Gt for the same forcing (Fig. 8a). Using the
357 HadGEM2-ES forcing, which is the same model used to force RACMO with α and γ set to their
358 best estimates (Fig. 4) gives 2000 Gt. We suggest that this may be the lower reasonable bound of
359 mass loss since the HadGEM-ES ocean temperatures rise notably slower than the ensemble mean
360 (Fig. 6). Note that all 3 simulations of front position (Fig 7C, Fig. 8) show a relatively stable position
361 around 18 km upstream from its 2013 location. Examination of the change in velocities during the
362 simulation (Fig. 9) suggests that the explanation for this stability is strong flow convergence near
363 the future glacier front that largely offsets dynamic thinning. Notice that the South side of the fast-
364 flow-area in 20th century was quite close to ice-free land, while in later half of this century
365 convergent flow in the South is fed by a substantial area of ice stream.

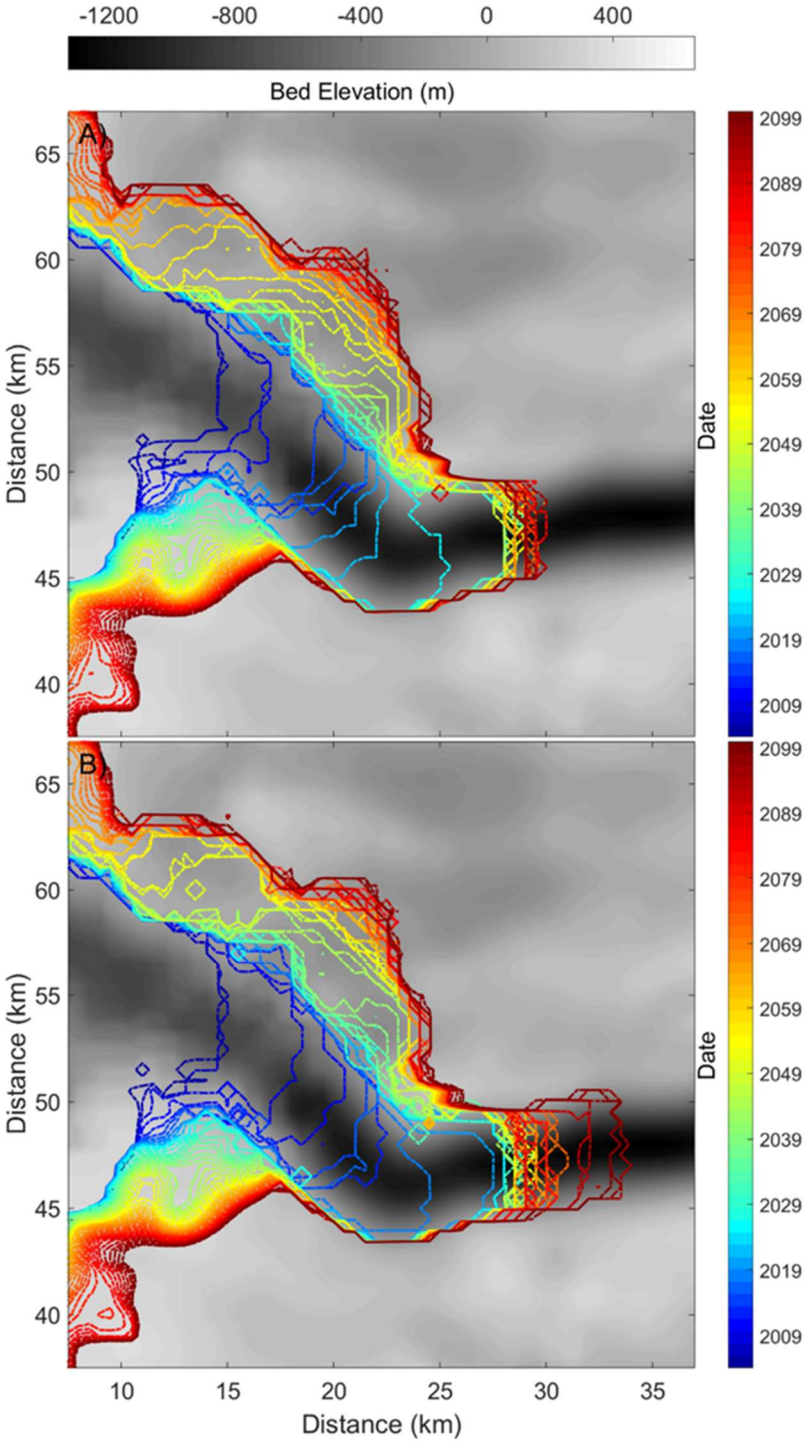

366

367 **Figure 8. Upper and lower estimates of July front positions within this century with colors**
368 **indicating the date (color bar) for A) lower bound with scalings of (1,0.8) and the HadGEM-ES**
369 **forcing B) upper bound of mass loss projection with (α, γ) parameter scalings of (1.2,1), and the**
370 **7-model ensemble climate forcing.**

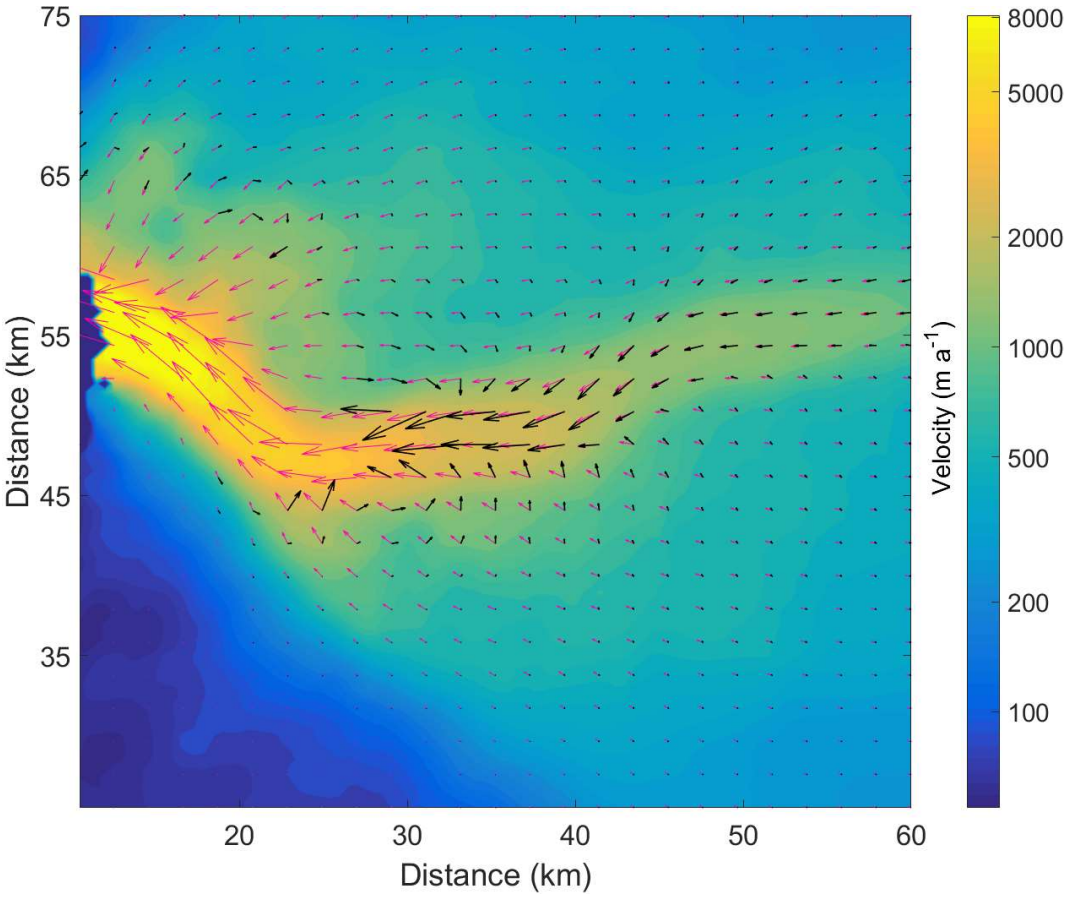

Figure 9. Simulated velocity vectors in 2004 (pink vectors) with their magnitudes (right color bar) and velocity difference between 2004 and 2099 (2099's minus 2004's, black vectors), for clarity vector lengths are clipped at 5 km a^{-1}.

Exploring the (α, γ) scaling parameter space we notice that values of (1.0, 0.8) produce a mass loss over this century of 2021 Gt with the HadGEM-ES ocean forcing, almost the same value as for the best set of parameters. This implies that less submarine melting (determined by γ) leads to larger ice loss by dynamic processes. The reason is that lesser submarine melt allows a larger ice thickness at the grounding line with stronger dynamic thinning in advancing season. Notice in our stress balance equation (Eq. 3), thickness contributes to driving force term, thus ice flux across the grounding line is highly nonlinear in ice thickness. This highly nonlinear relationship is also shown in our sensitivity tests (Fig. 4). Over the mismatch field measured by front velocity (Fig. 4, Panel B), the velocity is partly dominated by low values of γ scaling around the scaling line for α = 1.06, while α

is almost the only control on velocity over the region where scaled α<1.09. Within our sample space, the non-linear and non-monotonic relationship between submarine melting and retreats is clear (Fig. 4, Panel A). Around the point of scalings (α = 1.12, γ = 1.0), total retreat will increase no matter if γ is decreasing or increasing within the scaling range $0.8 < \gamma < 1.2$. The area where scaled $\alpha > 1.0$ in sample space is the very likely future condition for Jakobshavn Isbræ because increasing terminal ice cliff height caused by retreating into deep water will act as an amplifier to frontal driving force.

4 Discussion

4.1 Parameterization of Buttressing effect

The sudden 1.1℃ rise in temperature of water entering Ilulissat fjord in 1997 (Holland et al., 2008) initiated rapid melting and disintegration of the ice shelf in 2003. This disintegration coincided with a near doubling of ice velocities. Modeling (Vieli et al., 2011) suggested that this was due to the reduction in buttressing from the ice-mélange. We can realistically reproduce the velocity variation of Jakobshavn Isbræ on seasonal and inter-annual scales using our parameterization of the buttressing effect from the ice mélange in the fjord.

Gladish et al. (2015) analyzed glacial flow speeds from 1998 to 2014, finding no correlation with Ilulissat fjord temperatures. This is because at the beginning of 2004, Jakobshavn's evolution entered a new phase with the disintegration of the ice shelf. We find good correlations between Disko Bay temperatures and ice velocities from 2004 to 2014. The improvement in correlation with temperatures may be explained by a faster response between the grounded glacier and the fjord water temperatures after loss of the floating ice shelf.

Buttressing would affect the calving process by altering the longitudinal resistive stress in the glacier.

405 Temperatures in Ilulissat Fjord will be warmer during the 21st century under essentially all climate
406 scenarios, even those with modest emissions, due to the thermal inertia of the oceans. Thus a new
407 floating ice shelf is unlikely to form. Prior to 2004, there were large changes in Jakobshavn: loss of
408 ~15 km long ice shelf and the sudden rise in fjord temperatures in 1998. There are fewer mechanisms
409 to effect such dramatic changes in the future now that almost the entirety of the glacier is grounded.
410 We therefore propose that our representation of the mélange buttressing mechanism, tuned for 2004-
411 2013, is likely to maintain its validity during the 21st century.

412 4.2 Horizontal shearing and viscosity

413 Van Der Veen et al. (2011) estimated a maximum horizontal shear stress of ~800 kPa across the
414 shear margin of Jakobshavn Isbræ where the horizontal velocity shear reaches the peak, while the
415 bed stress is only 10-40 kPa in fast flowing regions (Shapero et al., 2016). Given that the width of
416 the Jakobshavn Isbræ fast flow region is typically under 5 km and its thickness is typically between
417 1-2 km, these numbers indicate that the shear margins provide at least an order of magnitude greater
418 total resistance than the bed. Thus, the shear margin, rather than the bed of Jakobshavn Isbræ
419 provides most of the resistance balancing the driving force. The main trunk of Jakobshavn Isbræ
420 exhibits considerable seasonal velocity changes, while the slow moving ice outside the shear margin
421 has little or no seasonal cycle. This flow structure implies speed gradients perpendicular to the flow
422 direction with large seasonal variation. These velocity shears would in turn generate large seasonal
423 variations in effective ice viscosity (Eq. 6). This mechanism is due to the non-linear rheology of the
424 ice in the fast flow region: increases in the speed of fast flowing ice cause increases in horizontal
425 shear stress across the margins, reduced viscosity, and further increased horizontal velocity shear,
426 allowing further increase to speeds in the fast flow region. Observations show that, as the terminus
427 retreated into deeper water, seasonal fluctuations in terminus velocity increased (Joughin et al. 2008).

By 2012, the summer time peak terminus velocity was ~ 17 km a^{-1}, more than twice the wintertime minimum velocity (Joughin et al. 2014). This amplified seasonal velocity cycle was likely enhanced by the shear-margin weakening mechanism.

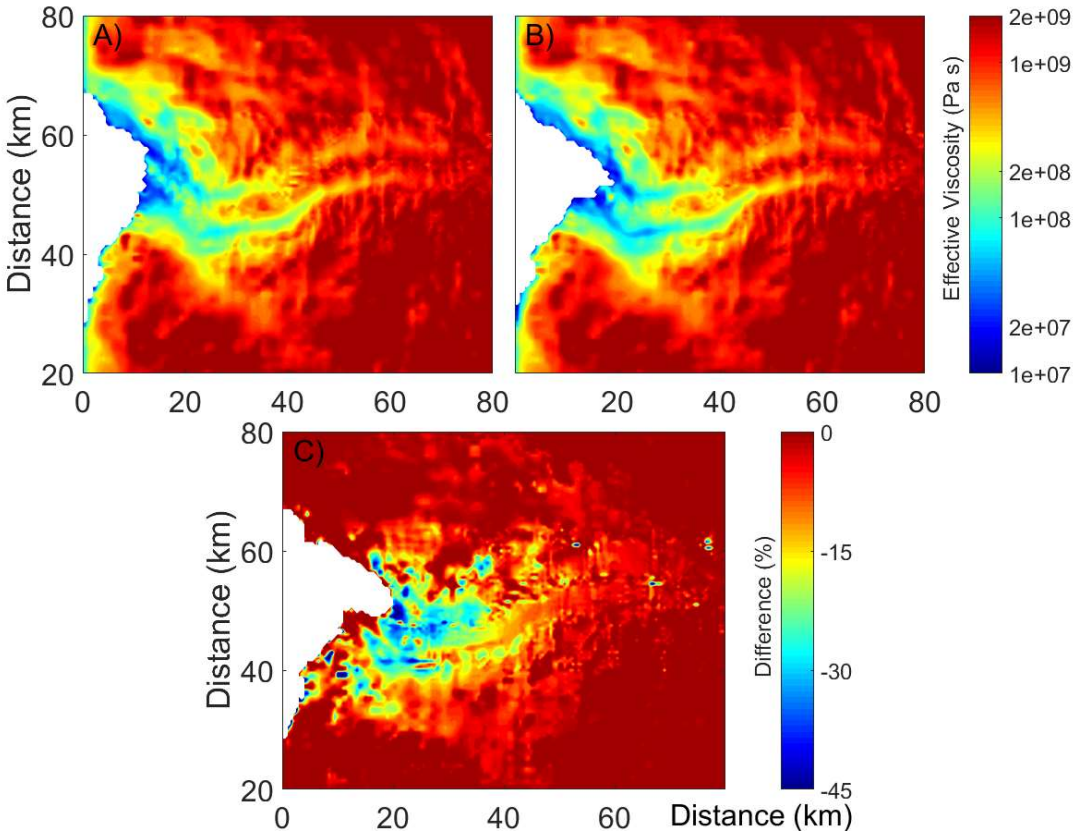

Figure 10. Modeled annual mean of vertically averaged effective viscosity $\Phi\mu$ (Eq. 5) in 2004 (A) and 2013 (B) and the percentage decreases from 2004 to 2013 (C).

Our modeled shear margin weakening on decadal scales is consistent with other estimates from a thermomechanical ice flow model of Jakobshavn Isbræ forced by calving front positions (Bondzio et al., 2017). Their modeled viscosity drops between 2003 to 2015 reach ~ 40% which is close to our maximum viscosity decrease of ~ 45% between 2004 to 2013 (Fig. 10). The extreme calving season we simulated in summer 2012 was accompanied by ~ 12 km a^{-1} variations in speed at the calving front, which were facilitated by the accompanying shear margin-induced ice viscosity

reductions of 60% at the time of maximum terminus advance. Simpler models of Jakobshavn Isbræ, using a flowband model (Nick et al., 2013) or simple calving parameterizations with no seasonal cycle (Muresan et al., 2016) cannot produce these seasonal variations in shearing. However, our model accommodates both the seasonal forcing from calving and the three-dimensional seasonal velocity shear impacts on effective viscosity. Without this physical process, speedups during intense calving events would be under-estimated, and this would lead to under-estimated mass transportation during the retreat. Bondzio et al. (2017) used a thermomechanical ice flow model to evolve the ice viscosity, which depends on a damage parameter that softens the ice in the shear margins. But their damage parameter also stays constant in time. Thus both the models of Bondzio et al., (2017) and ours only consider the contribution from strain rate weakening in time to evolving viscosity. Thermodynamics could play some role in changing viscosity, presumably if the ice temperatures increased over time, but our temperatures are fixed at -10°C.

Several processes absent from our model could affect ice viscosity. Crevasses saturated by surface melt water within the shear margins of Jakobshavn are visible on satellite images (Lampkin et al., 2013). This melt water can transfer heat throughout the ice column through discharge within crevasses and moulins thus softening the ice (Phillips et al., 2010). Incorporating a continuum damage model in BISICLES would further exaggerate the shear margin weakening as it raises the non-linear dependence of strain rates on stress fields (Sun et al., 2017).

4.3 Comparison with previous estimates

The cumulative mass change of Jakobshavn Isbræ estimated from airborne and satellite laser altimetry for 1997–2014 was tabulated Muresan et al. (2016). The mass loss over the 10-year period 2004-2013 modeled by Muresan et al. (2016) is closer to observations than ours (Table 1). This is partly due to different tuning targets: matching observed mass change was a stated target in their

study, whereas our study targets ice front position and velocity. Their close match to observed mass loss may be partly due to cancelling errors: 1) their modeled calving front barely moves after 2006, which leads to under-estimation of mass change; and 2) the modeled fast flow widths are larger than observations, which amplifies the mass flux across the calving front. These two biases will not always offset each other perfectly in the future.

Muresan et al. (2016) failed to simulate the retreat of Jakobshavn Isbræ after 2010. This may be due to the thickness threshold employed in their calving parameterization. Once Jakobshavn Isbræ terminus has retreated into the deeper part of the bedrock trough, the terminus height might never drop below their calving threshold of 375 m. In this case their calving rate will be solely due to the eigen parameterization of strain rates. Moreover, absence of seasonality in their calving front leads to under-estimated dynamic thinning, which is a key prerequisite for further calving. In contrast, our crevasse-depth calving model depends on stresses and surface water run-off with strong seasonal variation. As the terminus retreats and the surface slope steepens the enhanced surface stretching enhances the opening of crevasses in both calving parameterizations.

Nick et al. (2013) used a flow-band model to estimate a mass loss of 2280 Gt for Jakobshavn Isbræ by 2100 under the A1B climate scenario (Table 1). In our model we use RCP4.5 climate forcing, which has lower temperature rises than A1B, especially after 2050. Nick et al. (2013) prescribed a flow-band that has a near uniform width of 5 km near the terminus. Later modeling work using a similar model suggested that stability of the glacier is fundamentally controlled by geometry, and in reality the width varies along the ice-stream (Steiger et al. 2017). Nick et al. (2013) chose sets of parameters that produced small inter-annual retreats of Jakobshavn from 2000-2010, which may limit mass loss and retreat. The absence of the shear margin weakening feedback in their model also likely causes underestimation of mass loss. This could account for the comparable projected mass

loss to our results, and less terminus retreat (Table 1), even though their climate forcing scenario was warmer.

Another SSA model (Bondzio et al., 2018) projects larger retreats than ours, and uses a calving parameterization that predicts the location of calving depending on tensile stress distribution, regardless of ice thickness. In contrast our calving parameterization uses mélange buttressing effects and calving driven by seasonal filling of crevasses with surface water run-off, while Bondzio et al. (2018) drive their calving seasonality by a seasonal varying stress threshold. However, in the real world Jakobshavn, calving does not have to be of the full-thickness-type and can involve vertical motions (Xie et al., 2016) or the MICI (Marine Ice Cliff Instability) mechanism (Pollard et al., 2015), all of which are difficult to resolve by an SSA model. These calving types are probably becoming more and more important as it retreats into deep water. Therefore, we cannot confidently claim our crevasse-depth based calving parameterization is better than the calving criterion that only depends on tensile stress (Bondzio et al., 2018) for the future. In the next section we discuss how the model might be improved.

4.4 Model improvements

We overestimate mass loss relative to observations over Jakobshavn Isbræ drainage basin for 2004-2013 (Table 1). One reason for the discrepancy may be errors in initial ice thickness and real geometry in 2004. Excessive dynamic thinning was simulated over the lowest ~ 20 km of the main trunk due to over-estimated summer speed. For example, modeled front velocity soared to a peak of ~ 20 km a^{-1} in summer 2012, while the observed maximum speed is only 18 km a^{-1} (Joughin et al., 2014). In this summer, we simulated a series of full-thickness calving events that eventually left an unprecedented tall ice cliff. In reality, calving events do not always occur to full thickness, thus the glacier tends to form a shorter ice cliff that caters for lower velocity and less dynamic thinning.

509 Since the grounding line of Jakobshavn retreated to the bottom of a reverse bed slope in 2009, the
510 height of the calving front has generally increased, causing larger mass flux downstream across the
511 calving front. Instead of enhancing the seasonal fluctuation of calving front position, substantial
512 winter calving events have occurred instead. Given the fact that these calving events have reduced
513 the typical winter advance from ~ 6 km to ~ 3 km since 2010, winter calving is now likely as
514 important as summer run-off-driven calving. During this period of low magnitude seasonal
515 fluctuations, a series of retreats gradually moved the calving front position on inter-annual scale. In
516 contrast, the inter-annual retreats before 2009 were mostly driven by single calving seasons, e.g.,
517 May to July 2009. Our model using the Benn calving model is better able to simulate this earlier
518 retreat pattern, which is largely determined by each year's peak surface water run-off.

519 The grounding line of Jakobshavn Isbræ is unlikely to return to shallow water in the remainder of
520 the 21st century because bedrock elevations < - 1000 m beneath the main trunk further extend ~ 60
521 km inland. Accordingly, the latest retreat pattern including winter calving, is likely closer to the
522 pattern of future evolution of Jakobshavn Isbræ. A short floating part due to winter calving is always
523 accompanied by weaker lateral drag and steeper surface slope near the grounding line, all of which
524 are conducive for faster ice-flow. So, winter calving would enhance the downstream mass
525 transportation, a missing process in our model.

526 The process of winter calving must take place without any surface water. That calving must be
527 generated by processes affecting ice front stability, and that is likely due to changes at the base rather
528 than the surface. Evidence of calving by opening of basal crevasses and splitting comes from
529 terrestrial radar showing the terminus lifting several days prior to a large calving (Xie et al., 2016;
530 James et al., 2014). These observations suggest that the glacier is not in hydrostatic equilibrium
531 during calving. Our simulation specifies the glacier is in hydrostatic equilibrium on timescales of

the simulation. Our model cannot simulate the process of up-lifting. Instead we assume the upper and lower surface would instantly lift to the state of floating (Eq. 1). However, there is some evidence that Jakobshavn must behave super-buoyantly in winter. We observe that the simulated grounding line of Jakobshavn retreats even after cessation of calving front retreat (Fig. 3). These retreats can be explained by rapid dynamic thinning near the grounding line leading to its buoyancy exceeding gravity and, consequently, floating. Winter calving can occur in later winter (Cassotto et al., 2015) when calving front height is at its annual minimum and presumably at its least vulnerable to structural failure. Hence, MICI cannot explain this type of calving (Pollard et al., 2015). The existence of winter calving has greatly reduced the range of seasonal fluctuations in front position, which inhibited the growing of a temporary ice shelf that would buttress the grounded ice. Thus, lack of winter calving would cause underestimation of dynamic thinning as the glacier grows in winter.

A combination of discrete element model and continuum ice-dynamic model (solving the 3-Dimensional full-stokes equation) is able to reliably replicate observed calving styles in the case of a super-buoyant terminus (Benn et al. 2017). The discrete element model allows investigation of calving processes in unprecedented detail by analyzing the stress pattern dominated by glacier geometry and boundary conditions. However, these calving processes are beyond the capability of a calving parameterization based on surface crevasse depth assuming depth-independent flow. Better understanding of this buoyancy-driven calving and further model development to represent more details such as fracture propagation are needed to accurately simulate glacier's future evolution.

Ice thickness and basal topography with resolution of 150 m became available for main outlet glaciers of Greenland (Morlighem et al., 2017) recently (Fig. S3). This eases finer mesh resolution

to be used for modeling which then might reveal more details of ice-stream behavior especially perpendicular-to-flow direction, including more precise shear-margin-weakening and calving near side walls. Our assumption of simple Weertman basal drag (Eq. 7) may be improved by implementing a physics-based basal sliding law (Schoof, 2010; Gagliardini et al., 2014; Tsai et al., 2015), although basal drag accounts for only about 2% of present-day buttressing (Shapero et al., 2016). An improved sliding relation would likely produce more speedup and retreats in model results as dynamic thinning can reduce the effective pressure, leading to lower basal shear stress.

5 Conclusion

We use a three-dimensional dynamic ice-sheet model with a physically-based calving parameterization to model the evolution of Jakobshavn Isbræ. After tuning the parameters, our model can accurately reproduce Jakobshavn Isbræ's retreats and velocity changes from 2004-2013 on both seasonal and inter-annual scale. We project Jakobshavn Isbræ's future dynamic changes with climate forcing data from RACMO (2014-2099) and an ensemble mean of 7 Earth System Models for the RCP4.5 scenario.

We successfully model two-dimensional ice velocity and viscosity structures and their seasonal variations for Jakobshavn Isbræ, which are missing from several previous modeling studies. Moreover, capturing these two-dimensional structures allows us to handle the influence of horizontal velocity shear on effective ice viscosity, which impacts on speedup processes of Jakobshavn Isbræ.

We predict that Jakobshavn Isbræ's grounding line will retreat along the deep parts of a basal trough where bedrock elevation is significantly lower than at the present grounding line until about 2070. Retreat slows as the front reaches the deepest parts of the trough, but by the end of the century

acceleration is possible as the front passes that position. Using the current generation of calving parameterizations, which are essentially thickness threshold models, is challenging because of the increasing height of the calving front as Jakobshavn Isbræ retreats, meaning that crevasse penetration depths become too small to initiate calving. Our model successfully reproduced Jakobshavn Isbræ's retreat down a reverse bed slope with an elevation drop of ~ 400 m and the subsequent temporarily stable calving front position in 2013 and 2014.

Our results suggest that rapid dynamic thinning and calving caused by deep crevasse penetration are responsible for most of its recent mass loss, and will be decisive processes in future mass loss. Further exploration of the physics of calving and basal sliding of Greenland outlet glaciers are required to improve future projections.

Acknowledgements

This study is supported by National Key Research and Development Program of China (2018YFC1406104), National Key Science Program for Global Change Research (2015CB953601) and National Natural Science Foundation of China (No. 41506212). We thank Stephen Cornford for his help in implementing some parameterizations used in our model. Three referees provided very helpful suggestions on the model results. Rupert Gladstone is supported by Academy of Finland grant number 286587.

References

Alexander, P. M., and Luthcke, S. B.: Greenland Ice Sheet seasonal and spatial mass variability from model simulations and GRACE (2003-2012), The Cryosphere, 10(3), 1259, 2016.

Amundson, J. M., Fahnestock, M., Truffer, M., Brown, J., Lüthi, M. P., and Motyka, R. J.: Ice mélange dynamics and implications for terminus stability, Jakobshavn Isbræ, Greenland, J. Geophys. Res.-Earth Surf., 115(F1), 2010.

Bamber, J. L., Layberry, R. L., and Gogineni, S. P.: A new ice thickness and bed data set for the Greenland ice sheet: 1. Measurement, data reduction, and errors, J. Geophys Res.-Atmos, 106(D24), 33773-33780, 2001.

Benn, D. I., Åström, J., Zwinger, T., Todd, J., Nick, F. M., Cook, S., Hulton, N. R.J., and Luckman, A.: Melt-under-cutting and buoyancy-driven calving from tidewater glaciers: new insights from discrete element and continuum model simulations, J. Glaciol., 63(240), 691-702, 2017.

606 Benn, D. I., Warren, C. R., and Mottram, R. H.: Calving processes and the dynamics of calving
607 glaciers, Earth-Sci Rev., 82(3), 143-179, 2007.

608 Bentsen, M., Bethke, I., Debernard, J. B., Iversen, T., Kirkevåg, A., Seland, Ø., Drange, H., Roelandt,
609 C., Seierstad, I. A., Hoose, C., and Kristjánsson, J. E.: The Norwegian earth system model,
610 NorESM1-M-Part 1: Description and basic evaluation, Geosci. Model Dev., 5, 2843-2931, 2012.

611 Block, A. E., and Bell, R. E.: Geophysical evidence for soft bed sliding at Jakobshavn Isbrae, West
612 Greenland, The Cryosphere Discussions, 5, 339-366, 2011.

613 Bondzio, J. H., Morlighem, M., Seroussi, H., Kleiner, T., Rückamp, M., Mouginot, J., Moon, T.,
614 Larour, E. Y., and Humbert, A.: The mechanisms behind Jakobshavn Isbræ's acceleration and mass
615 loss: A 3-D thermomechanical model study, Geophys. Res. Lett., 44(12), 6252-6260, 2017.

616 Bondzio, J. H., Morlighem, M., Seroussi, H., Wood, M. H., and Mouginot, J.: Control of ocean
617 temperature on Jakobshavn Isbræ's present and future mass loss, Geophys. Res. Lett., 45(23), 12-
618 912, 2018.

619 Cassotto, R., Fahnestock, M., Amundson, J. M., Truffer, M., and Joughin, I.: Seasonal and
620 interannual variations in ice mélange and its impact on terminus stability, Jakobshavn Isbrae,
621 Greenland, J. Glaciol., 61(225), 76-88, 2015.

622 Collins, W. J., Bellouin, N., Doutriaux-Boucher, M., Gedney, N., Halloran, P., Hinton, T., Hughes,
623 J., Jones, C. D., Joshi, M., Liddicoat, S., Martin, G., O'Connor, F., Rae, J., Senior, C., Sitch, S.,
624 Totterdell, I., Wiltshire, A., and Martin, G.: Development and evaluation of an Earth-System model
625 HadGEM2, Geosci. Model Dev., 4(4), 1051-1075, 2011.

626 Cornford, S. L., Martin, D. F., Graves, D. T., Ranken, D. F., Le Brocq, A. M., Gladstone, R. M.,
627 Payne, A., J., Ng, E. G., and Lipscomb, W. H.: Adaptive mesh, finite volume modeling of marine
628 ice sheets, J. Comput. Phys., 232(1), 529-549, 2013.

629 Cornford, S. L., Martin, D. F., Payne, A. J., Ng, E. G., Le Brocq, A. M., Gladstone, R. M., Edwards,
630 T. L., Shannon, S. R., Agosta, C., Van Den Broeke, M. R., Hellmer, H. H., Krinner, G., Ligtenberg,
631 S. R. M., Timmermann, R., and Hellmer, H. H.: Century-scale simulations of the response of the
632 West Antarctic Ice Sheet to a warming climate, The Cryosphere, 9, 1-22, 2015.

633 Cowton, T. R., Sole, A. J., Nienow, P. W., Slater, D. A., and Christoffersen, P.: Linear response of
634 east Greenland's tidewater glaciers to ocean/atmosphere warming, P. Natl. Acad. Sci. USA, 115(31),
635 7907-7912, 2018.

636 Csatho, B., Schenk, T., Van Der Veen, C. J., and Krabill, W. B.: Intermittent thinning of Jakobshavn
637 Isbrae, West Greenland, since the little ice age, J. Glaciol., 54(184), 131-144, 2008.

638 Cuffey, K. M., and Paterson, W. S. B.: The physics of glaciers. Academic Press, 2010.

639 Dee, D., Uppala, S., Simmons, A., Berrisford, P., Poli, P., Kobayashi, S., Andrae, U., Balmaseda,
640 M., Balsamo, G., Bauer, P., Bechtold, P., Beljaars, A. C. M., van de Berg, L., Bidlot, J., Bormann,
641 N., Delsol, C., Dragani, R., Fuentes, M., Geer, A. J., Haimberger, L., Healy, S. B., Hersbach, H.,
642 Hólm, E. V., Isaksen, L., Kållberg, P., Köhler, M., Matricardi, M., McNally, A. P., Monge-Sanz, B.
643 M., Morcrette, J. J., Park, B. K., Peubey, C., de Rosnay, P., Tavolato, C., Thépaut, J. N., and Vitart,
644 F.: The ERA-Interim reanalysis: Configuration and performance of the data assimilation system, Q.
645 J. Roy. Meteor. Soc., 137, 553–597, 2011.

Dufresne, J. L., Foujols, M. A., Denvil, S., Caubel, A., Marti, O., Aumont, O., Balkanski, Y., Bekki, S., Bellenger, H., Benshila, R., Bony, S., Bopp, L., Braconnot, P., Brockmann, P., Cadule, P., Cheruy, F., Codron, F., Cozic, A., Cugnet, D., De Noblet, N., Duvel, J. P., Eth´e, C., Fairhead, L., Fichefet, T., Flavoni, S., Friedlingstein, P., Grandpeix, J. Y., Guez, L., Guilyardi, E., Hauglustaine, D., Hourdin, F., Idelkadi, A., Ghattas, J., Joussaume, S., Kageyama, M., Krinner, G., Labetoulle, S., Lahellec, A., Lefebvre, M. P., Lefevre, F., Levy, C., Li, Z. X., Lloyd, J., Lott, F., Madec, G., Mancip, M., Marchand, M., Masson, S., Meurdesoif, Y., Mignot, J., Musat, I., Parouty, S., Polcher, J., Rio, C., Schulz, M., Swingedouw, D., Szopa, S., Talandier, C., Terray, P., Viovy, N., and Bony, S.: Climate change projections using the IPSL-CM5 Earth System Model: from CMIP3 to CMIP5, Clim. Dynam., 40(9-10), 2123-2165, 2013.

Gagliardini, O., Passalacqua, O., and Werder, M. A.: Retroactions between Basal Hydrology and Basal Sliding from Numerical Experiments. In AGU Fall Meeting Abstracts, 2014.

Giorgetta, M. A., Jungclaus, J., Reick, C. H., Legutke, S., Bader, J., Böttinger, M., Brovkin, V., Crueger, T., Esch, M., Fieg, K., Glushak, K., Gayler, V., Haak, H., Hollweg, H., Ilyina, T., Kinne, S., Kornblueh, L., Matei, D., Mauritsen, T., Mikolajewicz, U., Mueller, W., Notz, D., Pithan, F., Raddatz, T., Rast, S., Redler, R., Roeckner, E., Schmidt, H., Schnur, R., Segschneider, J., Six, Katharina D., Stockhause, M., Timmreck, C., Wegner, J., Widmann, H., Wieners, K., Claussen, M., Marotzke, J., Stevens, B., and Glushak, K.: Climate and carbon cycle changes from 1850 to 2100 in MPI-ESM simulations for the Coupled Model Intercomparison Project phase 5, J. Adv. Model Earth Sy., 5(3), 572-597, 2013.

Gladish, C. V., Holland, D. M., Rosing-Asvid, A., Behrens, J. W., and Boje, J.: Oceanic boundary conditions for Jakobshavn Glacier. Part I: Variability and renewal of Ilulissat Icefjord waters, 2001-14, J. Phys. Oceanogr., 45(1), 3-32, 2015.

Gogineni, P. : CReSIS radar depth sounder data, Center for Remote Sensing of Ice Sheets, Lawrence, KS https://data.cresis.ku.edu, 2012.

Gordon, H. B., Rotstayn, L. D., McGregor, J. L., Dix, M. R., Kowalczyk, E. A., O'Farrell, S. P., Waterman, L. J., Hirst, A. C., Wilson, S. G., Collier, M. A., and Watterson, I. G.: The CSIRO Mk3 climate system model, 2002.

Habermann, M., Truffer, M., and Maxwell, D.: Changing basal conditions during the speed-up of Jakobshavn Isbræ, Greenland, The Cryosphere, 7(6), 1679-1692, 2013.

Holland, D. M., Thomas, R. H., De Young, B., Ribergaard, M. H., and Lyberth, B.: Acceleration of Jakobshavn Isbrae triggered by warm subsurface ocean waters, Nat. Geosci., 1(10), 659, 2008.

Howat, I. M., Ahn, Y., Joughin, I., van den Broeke, M. R., Lenaerts, J. T., and Smith, B.: Mass balance of Greenland's three largest outlet glaciers, 2000-2010, Geophys. Res. Lett., 38(12), 2011.

Jakobsson, M., Mayer, L., Coakley, B., Dowdeswell, J. A., Forbes, S., Fridman, B., Hodnesdal, H., Noormets, R., Pedersen, R., Rebesco, M., Schenke, H. W., Zarayskaya, Y., Accettella, D., Armstrong, A., Anderson, R. M., Bienhoff, P., Camerlenghi, A., Church, I., Edwards, M., Gardner, J. V., Hall, J. K., Hell, B., Hestvik, O., Kristoffersen, Y., Marcussen, C., Mohammad, R., Mosher, D., Nghiem, S. V., Pedrosa, M. T., Travaglini, P. G., and Schenke, H. W.: The international bathymetric chart of the Arctic Ocean (IBCAO) version 3.0, Geophys. Res. Lett., 39(12), 2012.

James, T. D., Murray, T., Selmes, N., Scharrer, K., and O'Leary, M.: Buoyant flexure and basal crevassing in dynamic mass loss at Helheim Glacier, Nat. Geosci., 7(8), 593-596, 2014.

Ji, D., Wang, L., Feng, J., Wu, Q., Cheng, H., Zhang, Q., Yang, J., Dong, W., Dai, Y., Gong, D., Zhang, R., Wang, X., Liu, J., Moore, J. C., Chen, D., and Zhang, R. H.: Description and basic evaluation of Beijing Normal University Earth system model (BNU-ESM) version 1, Geosci. Model Dev., 7(5), 2039-2064, 2014.

Joughin, I., Abdalati, W., and Fahnestock, M.: Large fluctuations in speed on Greenland's Jakobshavn Isbrae glacier, Nature, 432(7017), 608, 2004.

Joughin, I., Howat, I. M., Fahnestock, M., Smith, B., Krabill, W., Alley, R. B., Stern, H., and Truffer, M.: Continued evolution of Jakobshavn Isbrae following its rapid speedup, J. Geophys. Res.-Earth Surf., 113(F4), 2008.

Joughin, I., Smith, B. E., and Howat, I. M.: A complete map of Greenland ice velocity derived from satellite data collected over 20 years, J. Glaciol., 64(243), 1-11, 2018.

Joughin, I., Smith, B. E., Howat, I. M., Scambos, T., and Moon, T.: Greenland flow variability from ice-sheet-wide velocity mapping, J. Glaciol., 56(197), 415-430, 2010.

Joughin, I., Smith, B., Shean, D., and Floricioiu, D.: Brief communication: Further summer speedup of Jakobshavn Isbræ, The Cryosphere, 8, 209-214, 2014.

Krabill, W., Abdalati, W., Frederick, E., Manizade, S., Martin, C., Sonntag, J., Swift, R., Thomas, R., Wright, W., and Yungel, J.: Greenland ice sheet: High-elevation balance and peripheral thinning. Science, 289(5478), 428-430, 2000.

Lampkin, D. J., Amador, N., Parizek, B. R., Farness, K., and Jezek, K.: Drainage from water-filled crevasses along the margins of Jakobshavn Isbræ: A potential catalyst for catchment expansion, J. Geophys. Res.-Earth Surf., 118(2), 795-813, 2013.

Luckman, A., and Murray, T.: Seasonal variation in velocity before retreat of Jakobshavn Isbræ, Greenland, Geophys. Res. Lett., 32(8), 2005.

Morlighem, M., Williams, C. N., Rignot, E., An, L., Arndt, J. E., Bamber, J. L., Catania, G., Chauché, N., Dowdeswell, J. A., Dorschel, B., Fenty, I., Hogan, K., Howat, I., Hubbard, A., Jakobsson, M., Jordan, T. M., Kjeldsen, K. K., Millan, R., Mayer, L., Mouginot, J., Noël, B. P. Y., O'Cofaigh, C., Palmer, S., Rysgaard, S., Seroussi, H., Siegert, M. J., Slabon, P., Straneo, F., Van den Broeke, M. R., Weinrebe, W., Wood, M., and Zinglersen, K. B.: BedMachine v3: Complete bed topography and ocean bathymetry mapping of Greenland from multibeam echo sounding combined with mass conservation, Geophys. Res. Lett., 44(21), 11-051, 2017.

Moss, R. H., Edmonds, J. A., Hibbard, K. A., Manning, M. R., Rose, S. K., Van Vuuren, D. P., Carter, T. R., Emori, S., Kainuma, M., Kram, T., Meehl, G. A., Mitchell, J. F.B., Nakicenovic, N., Riahi, K., Smith, S. J., Stouffer, R. J., Thomson, A. M., Weyant, J. P., and Wilbanks, T. J.: The next generation of scenarios for climate change research and assessment. Nature, 463(7282), 747-756, 2010.

Motyka, R. J., Truffer, M., Fahnestock, M., Mortensen, J., Rysgaard, S., and Howat, I.: Submarine melting of the 1985 Jakobshavn Isbræ floating mélange and the triggering of the current retreat, J. Geophys. Res.-Earth Surf., 116(F1), 2011.

Muresan, I. S., Khan, S. A., Aschwanden, A., Khroulev, C., Van Dam, T., Bamber, J., Van Den Broeke, M. R., Wouters, B., Munneke, P. K., and Kjær, K. H.: Modelled glacier dynamics over the last quarter of a century at Jakobshavn Isbræ, The Cryosphere, 10(2), 597-611, 2016.

729 Nick, F. M., Vieli, A., Andersen, M. L., Joughin, I., Payne, A., Edwards, T. L., Pattyn, F. and van de
730 Wal, R. S.: Future sea-level rise from Greenland's main outlet glaciers in a warming climate, Nature,
731 497(7448), 235, 2013.

732 Phillips, T., Rajaram, H., and Steffen, K.: Cryo-hydrologic warming: A potential mechanism for
733 rapid thermal response of ice sheets, Geophys. Res. Lett., 37(20), 2010.

734 Pollard, D., and DeConto, R. M.: Description of a hybrid ice sheet-shelf model, and application to
735 Antarctica, Geosci. Model Dev., 5(5), 1273, 2012.

736 Pollard, D., Deconto, R. M., and Alley, R. B.: Potential Antarctic ice sheet retreat driven by
737 hydrofracturing and ice cliff failure, Earth Planet. Sci. Lett., 412, 112-121, 2015

738 Schoof, C., and Hindmarsh, R. C.: Thin-film flows with wall slip: an asymptotic analysis of higher
739 order glacier flow models, Q. J. Mech. Appl. Math., 63(1), 73-114, 2010.

740 Shapero, D. R., Joughin, I. R., Poinar, K., Morlighem, M., and Gillet-Chaulet, F.: Basal resistance
741 for three of the largest Greenland outlet glaciers, J. Geophys. Res.-Earth Surf., 121(1), 168-180,
742 2016.

743 Sohn, H. G., Jezek, K. C., and van der Veen, C. J.: Jakobshavn Glacier, West Greenland: 30 years
744 of spaceborne observations, Geophys. Res. Lett., 25(14), 2699-2702, 1998.

745 Steiger, N., Nisancioglu, K. H., Åkesson, H., Fleurian, B. D., and Nick, F. M.: Simulated retreat of
746 Jakobshavn Isbræ since the Little Ice Age controlled by geometry, The Cryosphere, 12(7), 2249-
747 2266, 2018.

748 Sun, S., Cornford, S. L., Moore, J. C., Gladstone, R., and Zhao, L.: Ice shelf fracture
749 parameterization in an ice sheet model, The Cryosphere, 11(6), 2543-2554, 2017.

750 Tsai, V. C., Stewart, A. L., and Thompson, A. F.: Marine ice-sheet profiles and stability under
751 Coulomb basal conditions, J. Glaciol., 61(226), 205-215, 2015.

752 Van Angelen, J. H., M Lenaerts, J. T., Van den Broeke, M. R., Fettweis, X., and Meijgaard, E.: Rapid
753 loss of firn pore space accelerates 21st century Greenland mass loss, Geophys. Res. Lett., 40(10),
754 2109-2113, 2013.

755 Van Der Veen, C. J., Plummer, J. C., and Stearns, L. A.: Controls on the recent speed-up of
756 Jakobshavn Isbræ, West Greenland, J. Glaciol., 57(204), 770-782, 2011.

757 Vieli, A., and Nick, F. M.: Understanding and modelling rapid dynamic changes of tidewater outlet
758 glaciers: issues and implications, Surv. Geophys., 32(4-5), 437-458, 2011.

759 Watanabe, S., Hajima, T., Sudo, K., Nagashima, T., Takemura, T., Okajima, H., Nozawa, T., Kawase,
760 H., Abe, M., Yokohata, T., Ise, T., Sato, H., Kato. E., Takata, K., Emori, S., and Kawamiya, M.:
761 MIROC-ESM 2010: Model description and basic results of CMIP5-20c3m experiments, Geosci.
762 Model Dev., 4(4), 845, 2011.

763 Weertman, J.: On the Sliding of Glaciers, J. Glaciol., 3(21), 33-38, 1957.

764 Xie, S., Dixon, T. H., Voytenko, D., Holland, D. M., Holland, D., and Zheng, T.: Precursor motion
765 to iceberg calving at Jakobshavn Isbræ, Greenland, observed with terrestrial radar interferometry, J.
766 Glaciol., 62(236), 1134-1142, 2016.

Supplementary information

Simulated retreat of Jakobshavn Isbræ during the 21st century

Guo et al.

Correspondence to: X. Guo (xiaoran.guo@foxmail.com)

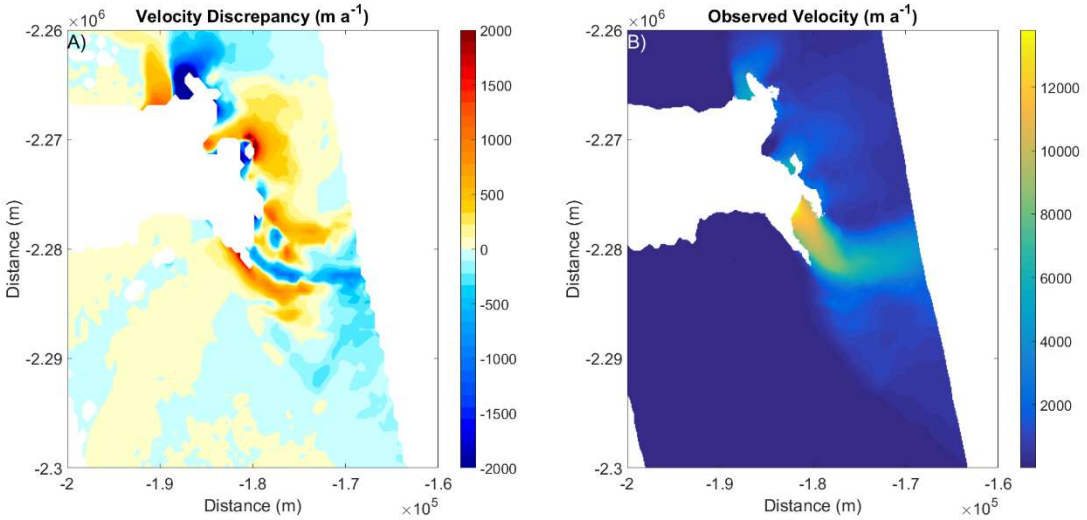

Figure S1. A) Velocity discrepancy (velocity from inversion - observed) and B) the observed velocity field (Joughin et al., 2010).

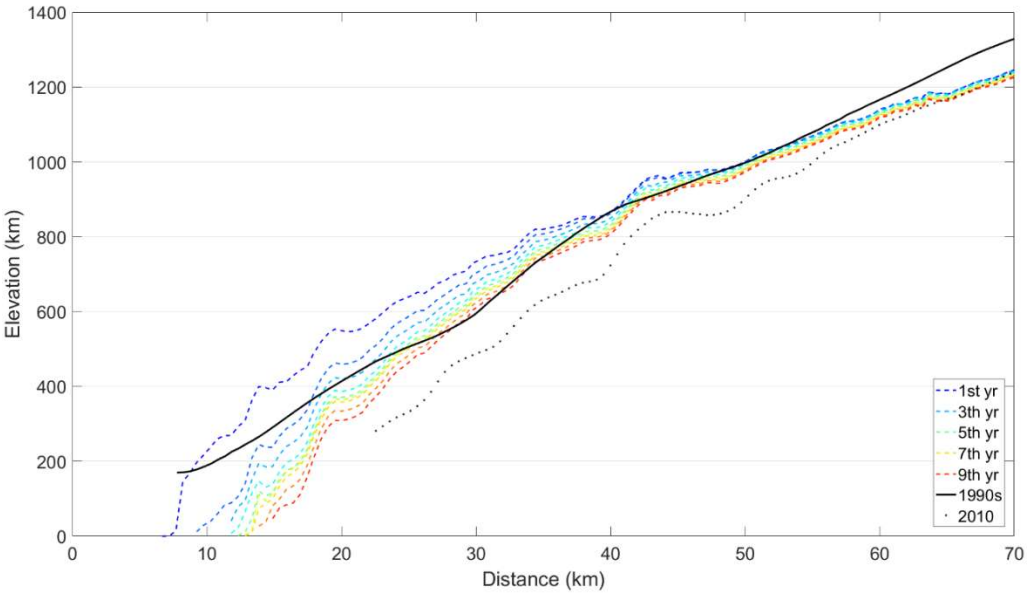

Figure S2. Profiles of surface elevation during the initialization procedure (section 2.3) step 3. Black solid line and black dashed line show the known profiles taken in the 1990s (Bamber et al., 2001) and 2010 (Gogineni et al., 2012) respectively. The profile with legend '1st yr' is the final state of section 2.3 step 2. The profile '7th yr' is the geometry rebuilt for 2004's Jakobshavn, which is the initial state for later simulations.

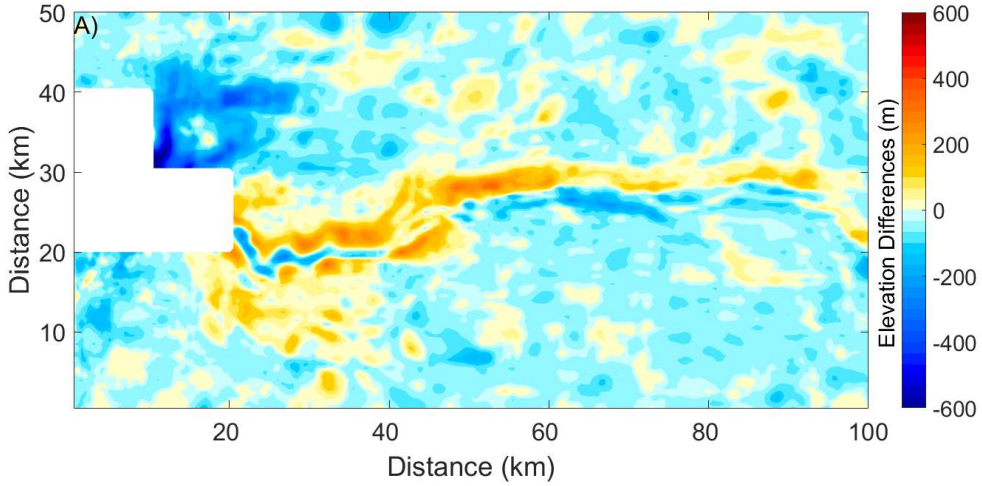

Figure S3. Bed elevation from BedMachine v3 (Morlighem et al., 2017) minus those from (Gogineni, 2012) used in this paper.